AEDC-TR-66-59

ARCHIVE COPY
DO NOT LOAN

OCT 20 1966

SPHERE DRAG MEASUREMENTS IN AN AEROBALLISTICS RANGE AT HIGH VELOCITIES AND LOW REYNOLDS NUMBERS

A. B. Bailey

ARO, Inc.

May 1966

Distribution of this document is unlimited.

PROPERTY OF U. S. AIR FORCE
AEDC LIBRARY
AF 40(600)1200

VON KÁRMÁN GAS DYNAMICS FACILITY
ARNOLD ENGINEERING DEVELOPMENT CENTER
AIR FORCE SYSTEMS COMMAND
ARNOLD AIR FORCE STATION, TENNESSEE

AEDC TECHNICAL LIBRARY
5 0720 00031 3742

NOTICES

When U. S. Government drawings specifications, or other data are used for any purpose other than a definitely related Government procurement operation, the Government thereby incurs no responsibility nor any obligation whatsoever, and the fact that the Government may have formulated, furnished, or in any way supplied the said drawings, specifications, or other data, is not to be regarded by implication or otherwise, or in any manner licensing the holder or any other person or corporation, or conveying any rights or permission to manufacture, use, or sell any patented invention that may in any way be related thereto.

Qualified users may obtain copies of this report from the Defense Documentation Center.

References to named commercial products in this report are not to be considered in any sense as an endorsement of the product by the United States Air Force or the Government.

SPHERE DRAG MEASUREMENTS IN AN AEROBALLISTICS RANGE AT HIGH VELOCITIES AND LOW REYNOLDS NUMBERS

A. B. Bailey
ARO, Inc.

Distribution of this document is unlimited.

AF - AEDC
Arnold AFB Tenn

FOREWORD

The research reported herein was sponsored by the Arnold Engineering Development Center (AEDC), Air Force Systems Command (AFSC), under Program Element 65402234.

The results of research presented were obtained by ARO, Inc. (a subsidiary of Sverdrup and Parcel, Inc.), contract operator of the AEDC, AFSC, Arnold Air Force Station, Tennessee, under Contract No. AF 40(600)-1200. The research was conducted from July 13, 1964 to April 1, 1965, under ARO Project No. VK3080, and the manuscript was submitted for publication on February 25, 1966.

The author wishes to acknowledge the assistance of C. J. Welsh in the performance of these experiments and the analysis of the results.

This technical report has been reviewed and is approved.

Conrad O. Forsythe
Captain, USAF
Aerospace Sciences Division
DCS/Research

Donald R. Eastman, Jr.
DCS/Research

ABSTRACT

The drag coefficients of spheres for $Re_2 > 10^4$ have been measured in the velocity range $3000 \leq V_\infty \leq 21,000$ ft/sec with an accuracy of approximately ±1.5 percent. In addition, successful techniques for manufacturing and launching ultralightweight spheres (densities approaching 1 lb/ft^3) have resulted in the ability to measure sphere drag coefficient in the velocity range $3000 \leq V_\infty \leq 12,000$ ft/sec and Reynolds number range $3 \leq Re_2 \leq 10^6$, with an accuracy of approximately ±4 percent. This wide range of operating conditions has made it possible to study the initial departures of sphere drag coefficient from the high Reynolds number, continuum level and also to make measurements at free-stream Knudsen numbers approaching 1.0. The results of the tests at the low Reynolds numbers are shown to be consistent with the results obtained in other low-density, hypersonic-flow facilities.

CONTENTS

		Page
	ABSTRACT	iii
	NOMENCLATURE	vi
I.	INTRODUCTION	1
II.	SPHERE DRAG MEASUREMENT	
	2.1 Method	2
	2.2 Lightweight Models	3
	2.3 Experimental Work	3
	2.4 Flow Properties	4
III.	DISCUSSION OF EXPERIMENTAL RESULTS	
	3.1 Sphere in Continuum Flow	5
	3.2 Sphere in the Transition Regime	7
IV.	CONCLUSIONS	11
	REFERENCES	12
	APPENDIX: Range K	31

ILLUSTRATIONS

Figure		
1.	A Comparison of Available Sphere Drag Coefficient Data at High Reynolds Numbers ($Re_2 \geq 10^4$) Obtained from Free-Flight Experiments	15
2.	Surface Pressure Distribution over a Sphere	
	a. Effect of Velocity	16
	b. Effect of Ambient Pressure	16
3.	Variation of Sphere Drag Coefficient with Velocity at High Reynolds Number ($Re_2 \geq 10^4$)	17
4.	Regimes of Rarefied Flow, According to Probstein (Ref. 17)	18
5.	Variation of Support-Free Sphere Drag Coefficient with Reynolds Number ($8 \leq M_\infty \leq 15$)	19
6.	Variation of Support-Free Sphere Drag Coefficient with Reynolds Number ($12.5 \leq M_\infty \leq 25$)	20
7.	Variation of Support-Free Sphere Drag Coefficient with Reynolds Number ($3 \leq M_\infty \leq 5$)	21

Figure		Page
8.	Variation of Support-Free Sphere Drag Coefficient with Reynolds Number ($5 \leq M_\infty \leq 8$).	22
9.	Variation of Support-Free Sphere Drag Coefficient with $\rho_2 V_2 d$ ($5 \leq M_\infty \leq 15$)	23

TABLE

I. Present Experimental Data 25

NOMENCLATURE

A	Constant, Eq. (14)
$a_0, a_1, \ldots$	Constants, Eq. (1)
C_D	Drag coefficient
C_{D_i}	Drag coefficient at infinite Reynolds number
C_p	Pressure coefficient
d	Diameter
Kn	Knudsen number, $2\lambda/d$
M	Mach number
m	Model mass
p	Pressure
Re	Reynolds number
S	Model cross-section area, $\pi d^2/4$
S_b	Mean molecular speed
T	Temperature
t	Time
V	Velocity
Z	Axial distance
γ	Ratio of specific heats
ϵ	Density ratio, ρ_∞/ρ_2

θ	Angle between the local normal to the surface and the direction of the undisturbed free-stream velocity
λ	Mean free path
μ	Viscosity
ρ	Density

SUBSCRIPTS

0	Isentropic stagnation conditions
2	Conditions immediately downstream of a normal shock in inviscid fluid, i. e., a Rankine-Hugoniot shock
i	Indicated impact pressure
m	A property of the sphere
STD	Conditions at 300°K and 760 mm Hg
w	Wall conditions
∞	Free-stream condition

SUPERSCRIPT

'	Conditions immediately downstream of a normal shock

SECTION I
INTRODUCTION

Sherman (Ref. 1) indicates that at this time the factor which has restricted the scope of experimental studies of rarefied flows has been the limited capability of the existing low-density wind tunnels. In order to cover the range of flow conditions from near-inviscid flow through the transition-flow regimes to near-free-molecule flow for a sphere in hypersonic flow, a wind tunnel must have a capability for wide variation of unit Reynolds number and/or model size, as well as hypersonic Mach number. The reason for this is that the transition regime for sphere drag covers the Knudsen number range from 0.01 to 10. At hypersonic Mach numbers the requirement of a large mean free path and a large test region is difficult to meet because of the rapid growth of the nozzle boundary layer and the severe pumping requirements. Most wind tunnels are designed to operate over a limited range of stagnation pressures, say one order of magnitude, so part of the variation in Knudsen number has to be achieved by varying model size. To date, very few experiments with low-density wind tunnels have varied model size by more than one order of magnitude, which means that any one wind tunnel can only produce data for a limited part of the transition-flow regime.

Despite these limitations, most of the data on drag of spheres in rarefied, hypersonic flow have been obtained in wind tunnels, e.g., Ref. 2. Although aeroballistic ranges would appear to be well suited to this particular measurement, limitations on both the lower pressure level attainable and the ability to accurately measure the drag (deceleration) of a high-speed sphere in a rarefied atmosphere have hindered the application of the aeroballistic range to the study of sphere drag at high Knudsen numbers.

The vacuum system of the Hypervelocity Pilot Range (Armament Test Cell, Hyperballistic (K)) can pump the range tank to a pressure of 0.001 mm Hg. In fact, the pressure can be held anywhere between 0.001 mm Hg and atmospheric pressure (1 psia ≡ 51.715 mm Hg). This corresponds to a mean free path variation from 2 to 2.6×10^{-6} in., which, for a 0.125-in.-diam sphere, corresponds to a Knudsen number range of $32 \lesssim Kn_\infty \lesssim 4.2 \times 10^{-5}$. Such a range of operating conditions should adequately cover the flow regimes from continuum to free-molecule flow.

In making measurements of sphere drag coefficient in an aeroballistic range, it is necessary to know the model weight, diameter, velocity, deceleration, range temperature, and range pressure. All of these quantities can be measured with considerable accuracy. It can be shown that

model deceleration is a function of the product of model diameter and density, together with the range pressure. The lowest pressure at which a measurable deceleration can be produced is determined by the instrumented length of the range and the lowest value of the product of model density and diameter that can be used. In Range K the smallest model that consistently can be detected and photographed is a 0.125-in.-diam sphere. This minimum model size, the 75 ft of instrumented range length, and the use of conventional model materials, e.g., steel, aluminum, and nylon, limit the lowest usable pressure to approximately 1 mm Hg. A successful technique for manufacturing and launching ultralightweight models, having densities down to 1 lb/ft^3, has been developed at VKF. This has extended the usable pressure range of Range K to pressures on the order of 0.01 mm Hg, and permits measurements of sphere drag over the Reynolds number range from 3 to 1 x 10^6. Additional information concerning Range K is contained in Appendix I.

SECTION II
SPHERE DRAG MEASUREMENT

2.1 METHOD

The longitudinal time-distance relationship of a model in free flight can be defined by a cubic equation in distance, viz,

$$t = a_0 + a_1 Z + a_2 Z^2 + a_3 Z^3 \tag{1}$$

This equation can be fitted to the measured time and distance values by the method of least squares.

The equation of motion of a body in free flight can be written as

$$m\, dV/dt = (1/2)\, \rho\, V^2 S\, C_D \tag{2}$$

or

$$C_D = 2m\,(dV/dt)\,/\,(\rho\, V^2 S) \tag{3}$$

Differentiating Eq. (1) and substituting in Eq. (3) gives

$$C_D = (4m/\rho\, S)(a_2/a_1) \tag{4}$$

For the present work, a program has been written for the IBM 7074 computer, which takes the model position data measured from the shadowgraphs using a Fairchild Film Reader and other relevant model and range data, and produces the model drag coefficient.

2.2 LIGHTWEIGHT MODELS

One of the limitations of the relatively short instrumented length (75 ft) and the few shadowgraph stations is that, in order to obtain a sufficiently accurate measurement of the model deceleration, a velocity drop of at least one percent of the initial velocity over the instrumented length is required. A study of Eq. (3) indicates that deceleration is given by

$$dV/dt \propto p/(\rho_m d) \tag{5}$$

if C_D, T, and V are assumed to be constant. Experience in Range K has indicated that a 0.125-in.-diam nylon sphere will have a velocity drop of one percent over the measured length at a pressure of approximately 1.5 mm Hg. Equation (5) shows that if the model density could be reduced from 70 lb/ft^3 (the density of nylon) to 1 lb/ft^3, and the drag coefficient remained unchanged, then such a model could be tested at a pressure of approximately 0.02 mm Hg.

An investigation into the feasibility of manufacturing and launching ultralight spheres (i.e., spheres having densities approaching 1 lb/ft^3) has shown that this can be accomplished satisfactorily. Models ranging in size from 0.125 to 1.75 in. in diameter have been successfully launched at velocities from 3000 to 16,000 ft/sec in the pressure range from 0.025 to 1.0 mm Hg. The material used in the manufacture of these models is a foamed plastic having the trade name Dylite®. These models were formed in an aluminum mold having a good surface finish, which was faithfully reproduced on the molded model. Static tests indicated that there were no measurable model deformations when these models were exposed to a high vacuum.

Some initial difficulties were experienced in launching the lightweight models. Most of these difficulties were found to be attributable to the method of separating the model and sabot. It was found that the pin and angled ramp type of stripper (see Appendix I) was the most satisfactory method of launching these models.

2.3 EXPERIMENTAL WORK

2.3.1 Conventional Testing

In this category of model testing the models were made of solid nylon, magnesium, aluminum, or stainless steel. A few firings were made with hollow, stainless steel models. All of this testing was carried out at pressures greater than 1 mm Hg and at velocities within the launcher operating envelope shown in Fig. I-1. Some of the data obtained

in this category of testing were taken in the course of other tests in Range K. This has, in some cases, resulted in the accumulation of many data points at one test condition and has provided a good opportunity to assess the degree of data repeatability.

2.3.2 Lightweight Models

The models used in this phase of testing were all foamed plastic and ranged in diameter from 0.125 to 0.437 in. All of this testing was carried out in the pressure range from 0.030 to 1.0 mm Hg for velocities between 3000 and 12,000 ft/sec. To minimize the possibility of range atmosphere contamination, and to avoid the need for lengthy pumping time between firings, the range was kept under a high vacuum for periods as long as one week. A summary of all the launchings made in support of this work is given in Table I.

2.4 FLOW PROPERTIES

2.4.1 Free-Stream Density

For the range atmosphere, one may write

$$\rho_\infty = \left(p_\infty / p_{STD}\right)\left(T_{STD} / T_\infty\right)\rho_{STD} \tag{6}$$

or

$$\rho_\infty = 9.01227 \times 10^{-4} \left(p_\infty / T_\infty\right) \text{ slugs/ft}^3 \tag{7}$$

where p_∞ and T_∞ are measured in mm Hg and °K, respectively.

2.4.2 Free-Stream Unit Reynolds Number

$$Re_\infty / \text{unit length} = \rho_\infty V_\infty / \mu_\infty$$

The free-stream viscosity for air is that given by Svehla in Ref. 3. Over a small temperature range (273 to 300°K) the variation of viscosity with temperature is adequately represented by the expression

$$\mu_\infty = \left[3.86 - 0.00963\left(T_\infty - T_{STD}\right)\right] \times 10^{-7} \text{ slugs/ft-sec} \tag{8}$$

Using this definition for viscosity, the free-stream unit Reynolds number may be written as

$$Re_\infty / \text{in.} = \left[751.02\left(p_\infty / T_\infty\right) V_\infty\right] / \left[3.86 + 0.00963\left(T_\infty - T_{STD}\right)\right] \tag{9}$$

2.4.3 Unit Reynolds Number Behind a Normal Shock Wave

$$Re_2 / \text{in.} = Re_\infty / \text{in.} \left(\mu_\infty / \mu_2\right) \tag{10}$$

The value of viscosity behind a normal shock wave, μ_2, is taken from Ref. 4, where the temperature T_2 required to define μ_2 is given in normal shock tables for air (Ref. 5).

SECTION III
DISCUSSION OF EXPERIMENTAL RESULTS

3.1 SPHERE IN CONTINUUM FLOW

A survey of the published data indicates that, for Reynolds numbers (based on conditions behind a normal shock wave) greater than 10^4, the sphere can be considered to be in the continuum, high-Reynolds-number flow regime, sometimes called the boundary-layer regime. Most of the available data from free-flight facilities (Refs. 6 through 11) are shown plotted in Fig. 1. Three of these sets of data were obtained with a conventional chronograph in the velocity measuring system (Refs. 6, 7, and 8). In Ref. 9 the projectile velocity and, hence, the model deceleration were measured with a system based on the use of a Fastax® camera. In the case of Ref. 10, the projectile time-distance information, from which drag coefficients were derived, was produced with a microwave resonant cavity. A ballistic pendulum has been used in the work reported in Ref. 11 for the derivation of sphere drag coefficient data. Three of these sets of data (Refs. 7, 9, and 10) were obtained with sabot-launched spheres, whereas the other three were obtained with bore-sized spheres. There are always problems of model deformation and weight loss when bore-size projectiles are used. Hodges (Ref. 6) has minimized the effect of weight loss by using the weight of the recovered projectile in his calculations of drag coefficient. At this time, however, it is not known what effect model deformation has on the drag coefficient. If these factors are ignored and the data derived from these six facilities are given equal merit, it will be seen that, for velocities greater than 6000 ft/sec, the sphere drag coefficient is constant and approximately equal to 0.92 when $Re_2 > 10^4$.

Let us consider the pressure drag of a sphere at high velocities, using the modified Newtonian pressure distribution:

$$C_p = C_{p_{max}} \cos^2 \theta \tag{11}$$

Integrating this over the front surface of the sphere, the sphere pressure drag coefficient can be written as

$$C_D = \frac{1}{\gamma_\infty M_\infty^2} \left(\frac{p_o'}{p_\infty} - 1 \right) \tag{12}$$

Using the real-gas relationships derived by Lewis and Burgess (Ref. 5), this equation has been evaluated at atmospheric pressure and is shown plotted in Fig. 1. Liu (Ref. 12) has calculated the pressure drag of a sphere using some simplification of the thermodynamic properties of air and his prediction also is shown in Fig. 1. Liu states that this theoretically predicted increase in drag coefficient with increase in Mach number is confirmed tentatively by Hodges' data (Ref. 6). Lampert (Ref. 13) corrected an error in Liu's analysis and showed that the theoretical, total sphere drag coefficient was approximately constant with a value of 0.96 over this velocity range. This is in good agreement with the value obtained from Eq. (12).

Lomax and Inouye (Ref. 14) recently have produced some theoretical pressure distributions for the front surface, i.e., the region bounded by the sonic line, of a high-speed sphere for a gas in equilibrium. Such distributions are directly applicable to the above free-flight sphere tests because all of these tests are at a sufficiently high pressure for the flow behind the normal part of the bow shock wave to be in equilibrium. These pressure distributions are compared with the Newtonian distribution in Fig. 2 for a range of velocities and pressures. It can be seen that the Newtonian pressure distribution will always overestimate the sphere pressure drag, and the indications are that, at a fixed ambient pressure, the pressure drag of a sphere will decrease with an increase of velocity. Since these published distributions (Ref. 14) do not extend over the entire front surface of the sphere, it is not possible to estimate the sphere pressure drag coefficient. However, Flugge-Lotz and Davis (Ref. 15) indicate that Lomax has provided them with a complete solution to the surface pressure distribution for a perfect gas (i.e., $\gamma = 1.4$) for $M_\infty = 10.0$. An integration of this pressure distribution gives a pressure drag coefficient of 0.89. Lomax and Inouye (Ref. 14) indicate that the pressure drag of a sphere in real gas will be less than that in a perfect gas. Therefore, it would be reasonable to conclude that the drag of a sphere in free flight at ambient pressures approaching one atmosphere will be close to a value of 0.89. Inspection of Fig. 2 also reveals that the surface pressure distribution is a weak function of ambient pressure at a fixed velocity, which would indicate that pressure drag coefficient is a weak function of the ambient pressure.

This review of the existing experimental and theoretical values of sphere drag at high speeds shows that there is some discrepancy between experiment and theory. The results of the present series of tests covering the velocity range from 3000 to 21,000 ft/sec are shown in Fig. 3. Also shown in Fig. 3 are some data obtained in the 1000-ft hypervelocity range (G) (Armament Test Cell, Hyperballistic (G)). The agreement between these results and those obtained in Range K is good.

It can be seen that all of the data presented in this figure have a spread of approximately ±1.5 percent. The best average curve through these data has been plotted in Fig. 1, where it is shown that the earlier test results are in agreement with the present results up to velocities of 6000 ft/sec. At the higher velocities, it is evident that the earlier results for C_D are too high. The agreement between the present data and what may be inferred from Lomax and Inouye's pressure distributions is encouraging and does confirm the theoretically predicted trends.

One of the problems associated with the determination of the continuum sphere drag coefficient is that of estimating the limiting Reynolds number above which it is safe to consider the flow to be near-inviscid or, in the present usage, continuum. For the purposes of this discussion, it has been assumed that continuum flow conditions exist for $Re_2 \geq 10^4$. This seems to be a reasonable assumption for the data obtained in the present series of tests. However, it must be remembered that for the present high-speed tests the wall-to-stagnation enthalpy ratio is always small, approximately 0.2 or less. Some results obtained in a wind tunnel where this ratio is on the order of 0.7 (Ref. 2) and $Re_2 \approx 10^4$ show a measured value of $C_D \approx 0.95$, as compared to a measured mean value of 0.885 in the present series of tests (see Fig. 3). The question then arises as to just what is the effect of wall temperature on the drag of a sphere at high Reynolds numbers? There may be another factor here, though, and that is the difficulty of correlating high-Mach-number, low-total-enthalpy data with high-Mach-number, true-total-enthalpy data. Attention has been drawn to this problem by Dayman (Ref. 16) and others.

3.2 SPHERE IN THE TRANSITION REGIME

The transition regime between continuum and free-molecule flow has been subdivided into various regimes depending upon the degree of rarefaction. The relevant definitions, based on criteria suggested by Probstein and Kemp (Ref. 17), in terms of Knudsen numbers for highly cooled, spherical bodies, are as follows:

		Ref. 17	Assumed in Fig. 4
Viscous layer	-	$2\lambda_\infty/d << \epsilon^{1/2}$	(0.01-0.03)
Incipient-merged layer	-	$2\lambda_\infty/d << 1$	(0.03-0.1)
Fully merged layer	-	$2\lambda_\infty/d < 1$	(0.1-1.0)
Transitional flow	-	$2\lambda_\infty/d \approx 1$	(1)

These regimes are shown in Fig. 4 for the model sizes covered in the present tests. This figure and the data contained in Table I indicate that the results of the present tests span the four flow regimes listed above.

It is generally assumed that the drag coefficient of a sphere in the flow regime where deviations from near-inviscid, continuum flow first begin can be considered to be the sum of two components.

$$C_D = C_{D_i} + C_{D_{S.F.}} \tag{13}$$

where C_{D_i} is the sphere drag coefficient at an infinite Reynolds number and $C_{D_{S.F.}}$ is the contribution caused by skin friction, which is itself, according to Davis and Flugge-Lotz (Ref. 15), a combination of the effects of vorticity, longitudinal curvature, transverse curvature, displacement, slip, and temperature jump. According to Ref. 15, the drag coefficient of a sphere may be written in the form

$$C_D = C_{D_i} + A/\sqrt{Re_2} + \ldots \tag{14}$$

With such an expression, it can readily be seen that, provided $A = 1$, there will be no significant deviations from the continuum drag coefficient for $Re_2 \geq 10^4$. This is one of the justifications for using this Reynolds number as the limit of continuum-flow (inviscid) conditions discussed in the preceding section.

Now it has been shown in Ref. 18 and in other reports listed there that, for values of Re_2 on the order of 100, the pressure at the stagnation point of a blunt body increases rapidly as the Reynolds number decreases below this value. Furthermore, in Ref. 19 it has been shown that the form of the surface pressure distribution does not change in a measurable manner, at least for $Re_2 \geq 100$. From this it can be concluded that the pressure component of drag will scale directly as the increase in stagnation point pressure.. In Ref. 18 it is shown that if shock-thickening effects are neglected the pressure at the stagnation point of a spherical body in hypersonic flow has the form

$$p_i/p_o' \approx 1 + 2\sqrt{2\epsilon}\,/\,\sqrt{Re_2} \tag{15}$$

Therefore, Eq. (14) would seem to have the proper form of the initial departure from continuum flow, in regard to both skin friction and pressure drag variations. For an ideal gas (where $\gamma = 1.4$) at high Mach numbers, $\epsilon \rightarrow 0.167$, whereas for a real gas, ϵ may be less than 0.167 and is a function of velocity and ambient conditions. Therefore, for a real gas the pressure at the stagnation point at a particular Reynolds number may be less than that for an ideal gas, though the difference is usually small.

From the foregoing discussion, it is evident that the Reynolds number used to correlate drag data in this regime is that based on conditions immediately downstream of a Rankine-Hugoniot type of normal shock wave. Sherman et al. (Ref. 20), in discussing methods of correlating data, consider a Reynolds number based on a free-stream density and velocity and a viscosity based on the stagnation temperature of the flow. Such a parameter is useful in test facilities where the stagnation temperature is known accurately. However, for free flight in an aeroballistic range at high ambient pressures and velocities, it becomes difficult to define the stagnation temperature because of a lack of thermodynamic data for these conditions.

The present data and those contained in Refs. 2, 21, and 22 are plotted in Fig. 5 using Re_2 as the relevant Reynolds number. In this comparison, only free-flight data are considered in order to eliminate any possible support interference effect upon sphere drag. The assumption made earlier that deviations from continuum flow can be expected when $Re_2 \leq 10^4$ is shown to be reasonable, as Fig. 5 shows that the first measurable deviations occur at a Reynolds number of approximately 4×10^3. The data from the three widely different facilities, i.e., shock tunnel, arc-heated tunnel, and free-flight range, are in reasonable agreement in the Reynolds number range where it is possible to compare the data. For the arc-heated wind tunnel of Ref. 2, it has been shown that the flow freezes essentially at the throat. For the present tests, the flow over the model for the low Reynolds number tests, i.e., $Re_2 < 10^3$, is in a state of nonequilibrium. These two results indicate that chemical kinetics may not have a significant effect upon sphere drag. The data presented in Ref. 21 are for micron-sized particles in two gases, air and argon. For these tests the flow over the model was certainly nonequilibrium. Although there is a random scatter in the latter data on the order of ±10 percent, the fact that data obtained in two different gases agree to this accuracy again appears to indicate that sphere drag is not a strong function of chemical kinetics effects.

A curve has been fitted to the results of the present tests, viz,

$$C_D = 0.882 + 1.4/\sqrt{Re_2} + 0.8/Re_2 \tag{16}$$

This is compared with one of the curves given in Ref. 2, viz,

$$C_D = 0.92 + 1.9/\sqrt{Re_2} - 0.7/Re_2 \tag{17}$$

Equation (16) may not be valid for $Re_2 \leq 10$ because, for Reynolds numbers in this region, it appears to overestimate the drag coefficient. This indicates that the fourth term in an equation of this form will be negative. The constants in Eq. (17) were based on an inviscid drag

coefficient of 0.92, from Hodges (Ref. 9), which has been shown in the present series of tests to be from 3 to 4 percent too high. A comparison of the present data and the theoretical calculations of Ref. 15 (Fig. 5) indicates a slight overestimate of drag by Eq. (17) in the region $Re_2 > 10^2$.

The data corresponding to $M_\infty \geq 12.5$ are shown plotted in Fig. 6. From these limited data and the results of Ref. 22, it does not appear that in the Mach number range $8 \leq M_\infty \leq 25$ there is a significant effect of Mach number on sphere drag coefficient.

In Figs. 7 and 8 some data obtained over the Mach number range $3 \leq M_\infty \leq 8$ are compared with those contained in Refs. 6, 7, 8, 23, and 24. In Fig. 7, a comparison of all the available free-flight cold-wall data in the speed range $3.0 \leq M_\infty \leq 4.8$ is made. These results obtained in several different facilities are in good agreement. The data in Ref. 24 were obtained in a conventional low-density, unheated-flow wind tunnel by cooling the spheres before dropping them into the test section. In the region of Reynolds number overlap, these data agree very well with the present results. In Fig. 8 a comparison of data in the speed range $5 \leq M_\infty \leq 8$ is made. From the limited aeroballistic range data at this speed, the variation of drag coefficient with Reynolds number does not appear to be any different from that shown in Fig. 5 for the speed range $8 < M_\infty < 12.5$. Thus the free-flight drag obtained in the low-density wind tunnel (Ref. 24) is larger than that obtained in the range when $5 \leq M_\infty \leq 8$. The lower speed data from these two facilities were in good agreement (cf Fig. 7); this indicates that the inherent accuracy of the two facilities is comparable, at least at lower Mach numbers. This then seems to imply that there may be more than simple, experimental error involved in the difference between data obtained in an unheated-flow, low-density wind tunnel and the free-flight range for $5 \leq M_\infty \leq 8.0$ when the data are correlated on the basis of Re_2.

To explore the possibility of there being another method of correlating hypersonic sphere drag data, the data contained in Figs. 5 and 8 are plotted against $\rho_2 V_2 d$ ($\equiv \rho_\infty V_\infty d$) in Fig. 9. The main result of this comparison is that the data of Ref. 24 are in good agreement with the other data when μ_2 is eliminated from the correlating parameter.

The fact that the data from these different facilities now correlate well in terms of $\rho_2 V_2 d$ implies that a viscosity based on a temperature common to all the tests is the valid one to use in the Reynolds number. For three of the sets of data, the wall temperature is approximately 300°K, whereas the cold wall data of Ref. 24 are for a wall temperature

of approximately 80°K. Even though there is one exception, it may tentatively be concluded from this that because three of the four sets of results seem to correlate well in terms of $\rho_2 V_2 d$ when the model wall temperature is approximately constant, then $\rho_2 V_2 d/\mu_w$ may be an equally significant parameter in this work. Such a parameter has previously been considered by Ashkenas (Ref. 25) in correlating low-density sphere drag measurements with equilibrium and nonequilibrium wall temperature. For the results considered in Ref. 25 this parameter did not appear to be wholly satisfactory.

SECTION IV
CONCLUSIONS

A comparison of the part of the present data obtained at large Reynolds numbers and high velocities with similar data obtained in other facilities indicates that, for velocities greater than 6000 ft/sec, the earlier results indicated a higher value of sphere drag coefficient than do the present results. The present data confirm that the drag coefficient is overestimated several percent by the modified Newtonian theory. In so doing, the present data confirm the validity of the detailed numerical solutions of Lomax and Inouye for both real and ideal gases in equilibrium. Their solutions further indicate that pressure drag is a weak function of velocity, a fact which is confirmed by the small, but measurable, decrease in drag coefficient in the speed range $6000 < V_\infty < 21,000$ ft/sec in the present data.

The tests carried out in the low Reynolds number range have proved that meaningful sphere drag coefficients can be obtained in a short (75-ft instrumented length) aeroballistic range at pressures on the order of 0.03 mm Hg. Such a capability has been made possible by the successful development of launching and manufacturing techniques for models having densities approaching 1 lb/ft^3. With one exception the sphere drag data from a wide variety of sources correlate well with the present data on the basis of Re_2, the Reynolds number based on conditions immediately downstream of a normal shock in an inviscid fluid. It has also been shown that, for the speed range of the present series of tests, deviations from high-Reynolds-number, continuum flow are first noticed at $Re_2 < 10^4$.

REFERENCES

1. Sherman, Frederick S. "Rarefied Gas Dynamics." Proceedings of the Third International Symposium on Rarefied Gas Dynamics. Vol. II, pp. 228-260. Academic Press, New York, 1963.

2. Kinslow, Max and Potter, J. L. "The Drag of Spheres in Rarefied Hypervelocity Flow." AEDC-TDR-62-205 (AD290519), December 1962.

3. Svehla, Roger A. "Estimated Viscosities and Thermal Conductivities of Gases at High Temperatures." NASA-TR-R-132, 1962.

4. Hansen, C. F. "Approximations for the Thermodynamic and Transport Properties of High-Temperature Air." NACA TN-4150, March 1958.

5. Lewis, Clark H. and Burgess, Ernest, G., III. "Charts of Normal Shock Wave Properties in Imperfect Air." AEDC-TDR-64-43 (AD433958), March 1964.

6. Hodges, A. J. "The Drag Coefficient of Very High Velocity Spheres." Journal of the Aeronautical Sciences, Vol. 24, No. 10, October 1957, pp. 755-758.

7. May, A. and Witt, A. "Free Flight Determinations of the Drag Coefficients of Spheres." Journal of the Aeronautical Sciences, Vol. 20, No. 9, September 1953, pp. 635-638.

8. Charters, A. and Thomas R. "The Aerodynamic Performance of Small Spheres from Subsonic to High Supersonic Velocities." Journal of the Aeronautical Sciences, Vol. 12, No. 4, October 1945, pp. 468-476.

9. Halperson, S., Boltz, P. T., and Hall, D. A. "High-Velocity-Projectile Drag Determination." Fourth Symposium on Hypervelocity Impact, APGC-TR-60-39 (III), April 1960.

10. Haislmaier, Robert J. "On Measuring Drag Coefficients in a Ballistic Range Using a Microwave Resonant Cavity." NOL TR 61-58, August 1961.

11. Clark, A. B. J. and Harris, F. T. "Free-Flight Air-Drag Measurement Techniques." Journal of the Aeronautical Sciences, Vol. 19, No. 6, June 1952, pp. 385-390.

12. Liu, V. C. "On the Drag of a Sphere at Extremely High Speeds." Journal of Applied Physics, Vol. 29, No. 2, February 1958, pp. 194-195.

13. Lampert, S. "Pressure Drag for a Sphere at Extreme Speeds." Journal of the Aerospace Sciences, Readers Forum, Vol. 28, No. 8, August 1961, p. 661.

14. Lomax, Harvard and Inouye, Mamoru. "Numerical Analysis of Flow Properties about Blunt Bodies Moving at Supersonic Speeds in an Equilibrium Gas." NASA TR-R-204, July 1964.

15. Davis, R. T. and Flugge-Lotz, I. "Second-Order Boundary-Layer Effects in Hypersonic Flow Past Axisymmetric Blunt Bodies." Journal of Fluid Mechanics, Vol. 20, Part 4, 1964, pp. 593-623.

16. Dayman, Bain, Jr. "Free Flight Hypersonic Viscous Effects on Slender Cones." AIAA Preprint No. 64-46 (A64-12968) (presented at the AIAA Aerospace Sciences Meeting, New York) January 1964.

17. Probstein, R. F. and Kemp, N. H. "Viscous Aerodynamic Characteristics in Hypersonic Rarefied Gas Flow." Journal of the Aero/Space Sciences, Vol. 27, No. 3, March 1960, pp. 174-192.

18. Potter, J. Leith and Bailey, Allan B. "Pressures in the Stagnation Regions of Blunt Bodies in the Viscous-Layer to Merged-Layer Regimes of Rarefied Flow." AEDC-TR-63-168 (AD416004), September 1963.

19. Bailey, A. B. and Sims, W. H. "The Shock Shape and Shock Detachment Distance for Spheres and Flat-Faced Bodies in Low-Density Hypervelocity Argon Flow." AEDC-TDR-63-21 (AD297197), February 1963.

20. Sherman, F. S., Willis, D. R. and Maslach, G. J. "Nearly Free Molecular Flow -- A comparison of Theory and Experiment." Institute of Engineering Research, University of California, Report No. AS-64-16, October 1964.

21. Slattery, J. C., Friichtenicht, J. F. and Hamermesh, B. "Interaction of Micrometeorites with Gaseous Targets." AIAA Journal, Vol. 2, No. 3, March 1964, pp. 543-548.

22. Geiger, R. E. "Some Sphere Drag Measurements in Low-Density Shock Tunnel Flows." GE R63SD23, July 1963.

23. May, Albert. "Supersonic Drag of Spheres at Low Reynolds Numbers in Free Flight." NAVORD R 4392, December 1956.

24. Aroesty, Jerome. "Sphere Drag in Low Density Supersonic Flow." University of California Report No. HE-150-192, January 1962.

25. Ashkenas, Harry. "Low-Density Sphere Drag with Equilibrium and Nonequilibrium Wall Temperature." Jet Propulsion Laboratory Technical Report No. 32-442, August 1963.

26. Maslach, G. J. "A Precision Differential Manometer." The Review of Scientific Instruments, Vol. 23, No. 7, July 1952, pp. 367-369.

27. Bailey, A. B. and Boylan, D. E. "Some Experiments on Impact-Pressure Probes in a Low-Density Hypervelocity Flow." AEDC-TN-61-161 (AD268391), December 1961.

28. Arney, G. D., Jr., and Bailey, A. B. "An Investigation of the Equilibrium Pressure Along Unequally Heated Tubes." AEDC-TDR-62-26 (AD272077), February 1962.

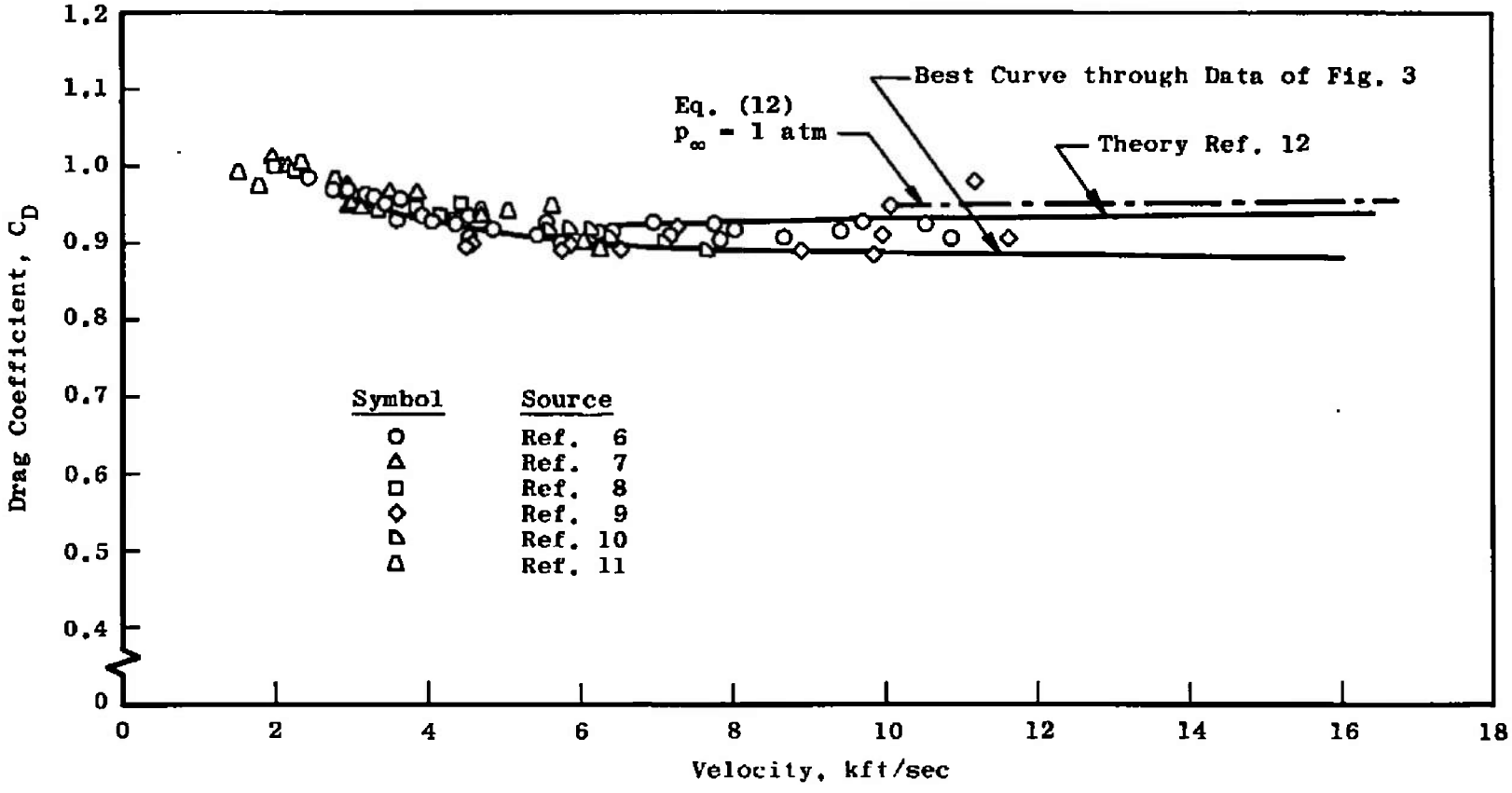

Fig. 1 A Comparison of Available Sphere Drag Coefficient Data at High Reynolds Numbers ($Re_2 \geq 10^4$) Obtained from Free-Flight Experiments

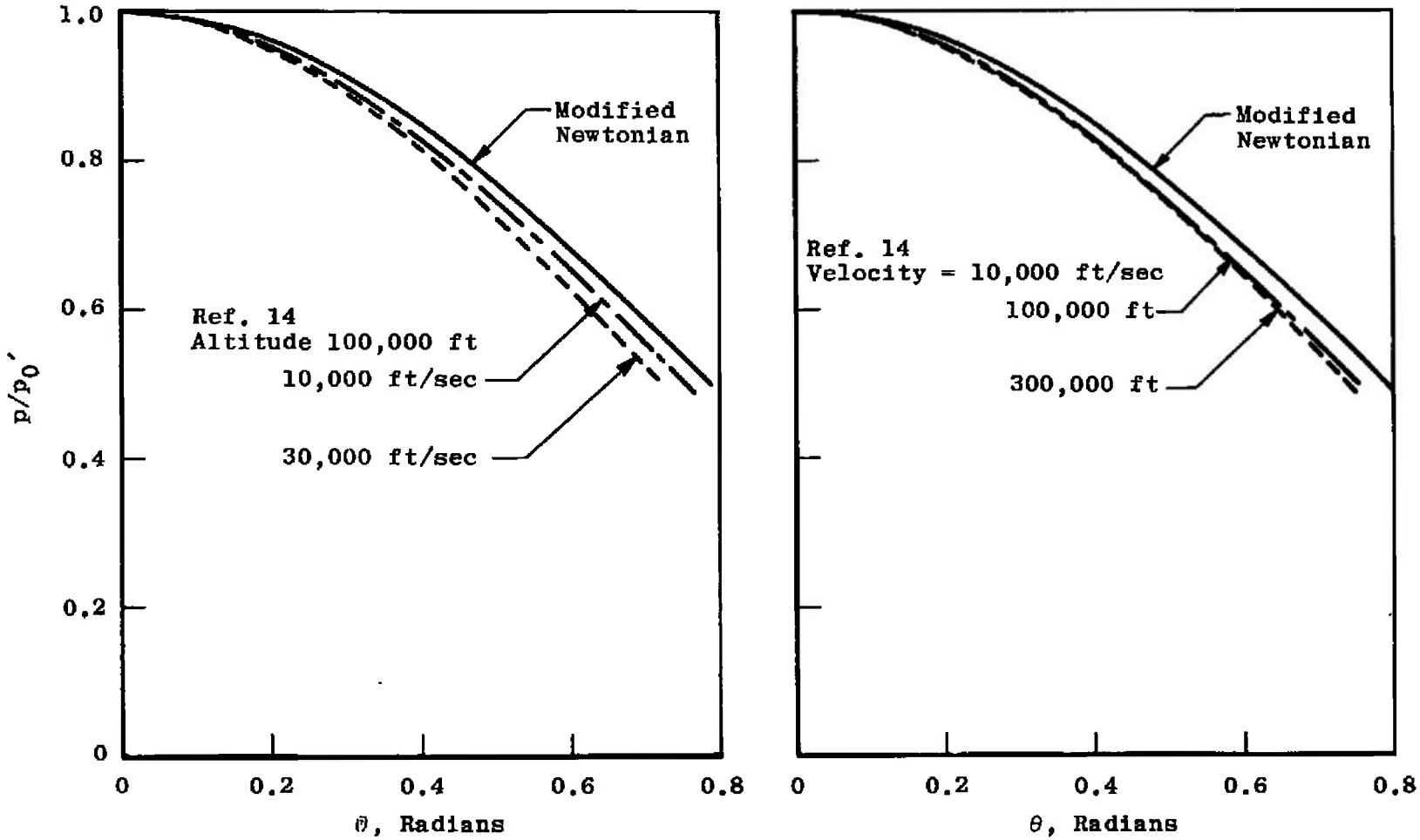

a. Effect of Velocity

b. Effect of Ambient Pressure

Fig. 2 Surface Pressure Distribution over a Sphere

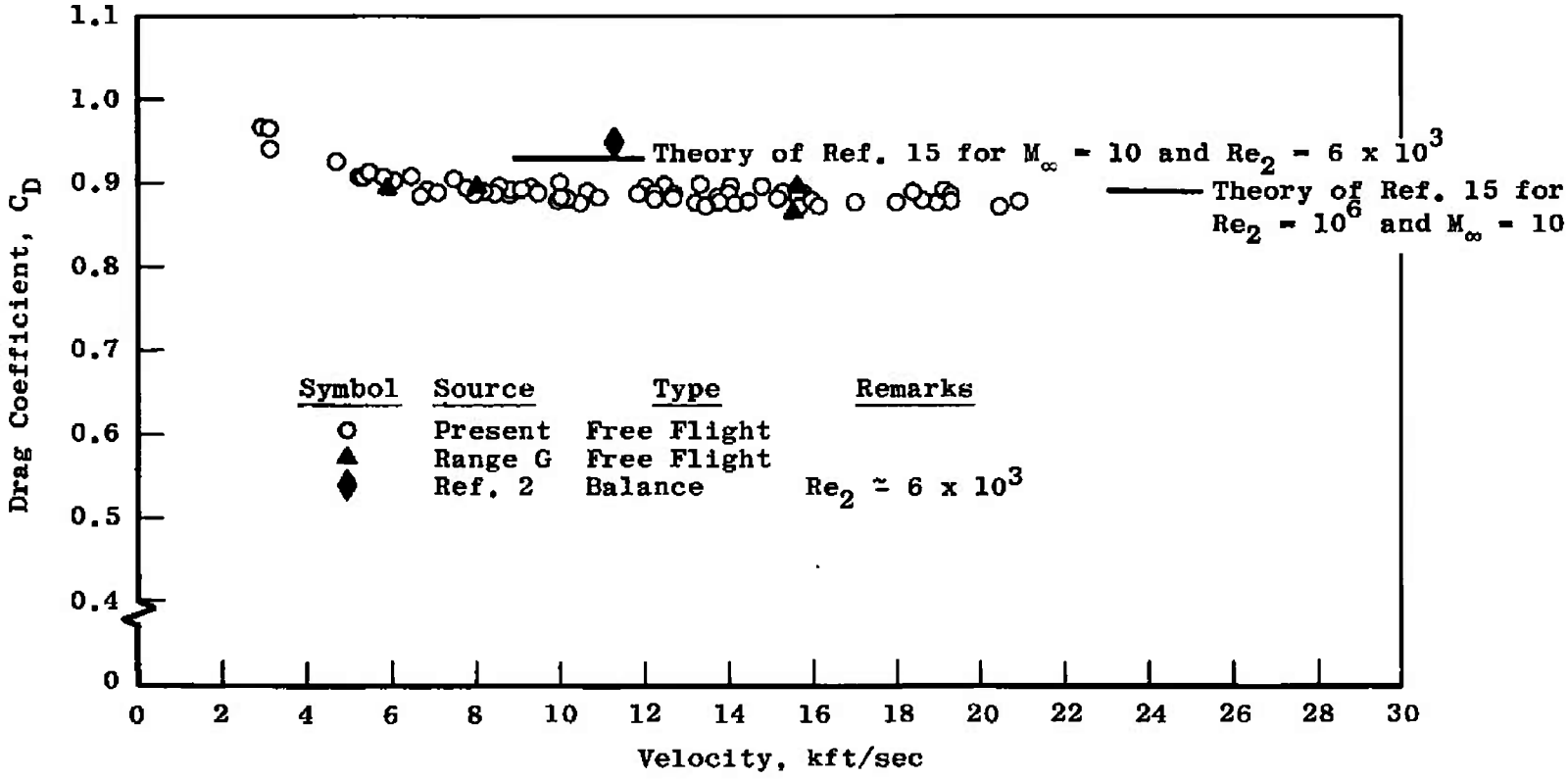

Fig. 3 Variation of Sphere Drag Coefficient with Velocity at High Reynolds Number ($Re_2 \geq 10^4$)

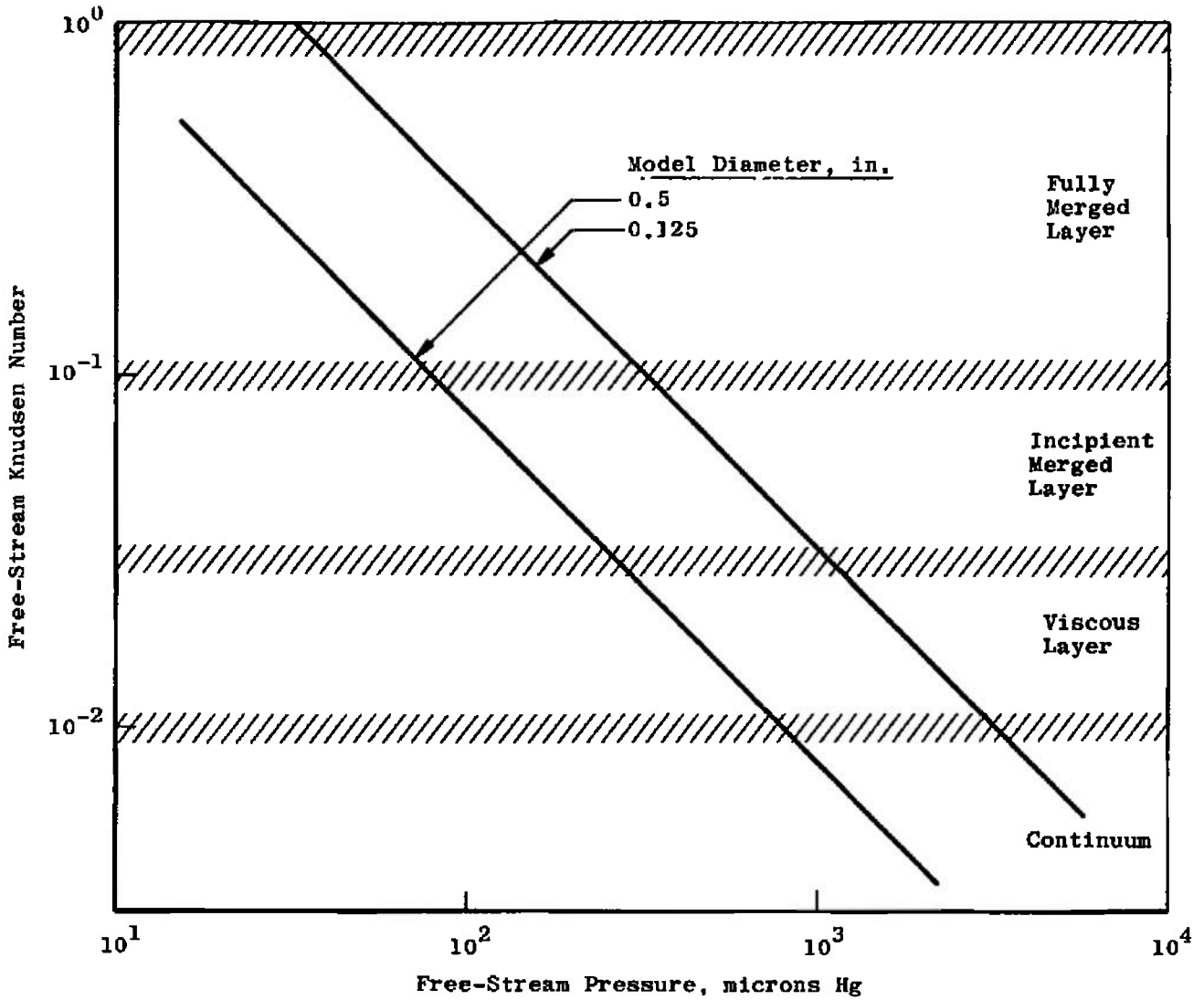

Fig. 4 Regimes of Rarefied Flow, According to Probstein (Ref. 17)

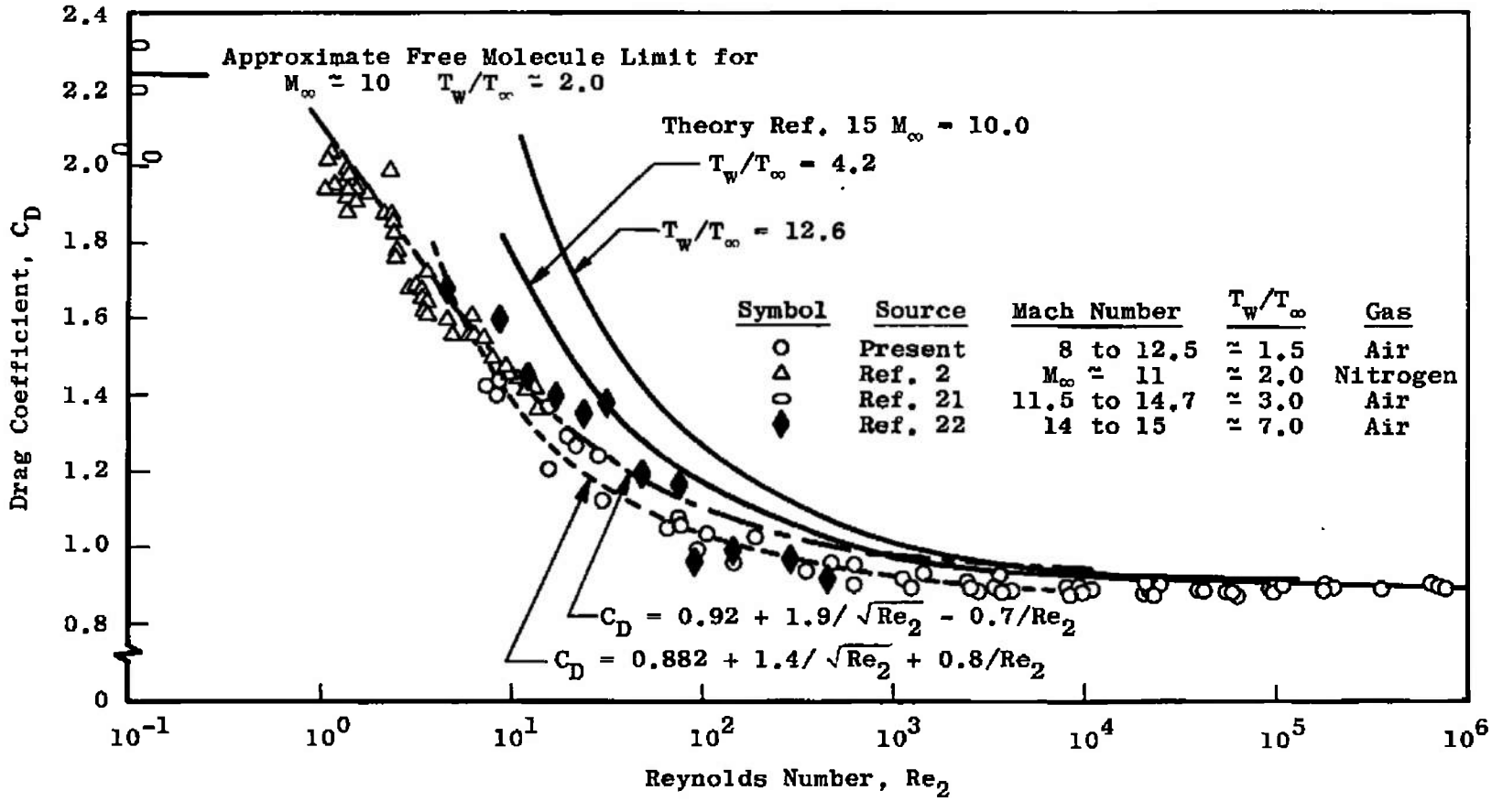

Fig. 5 Variation of Support-Free Sphere Drag Coefficient with Reynolds Number ($8 \leq M_\infty \leq 15$)

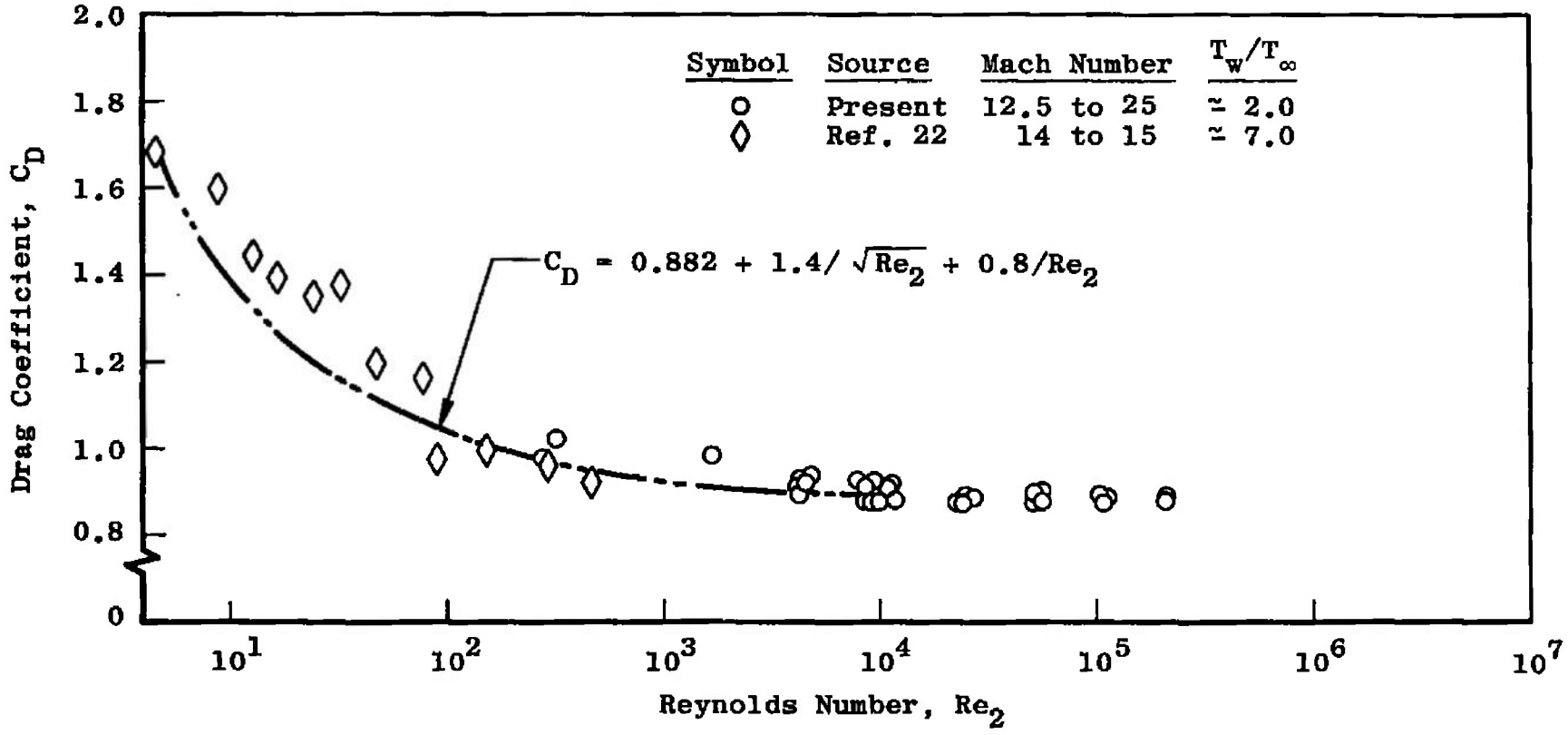

Fig. 6 Variation of Support-Free Sphere Drag Coefficient with Reynolds Number ($12.5 \leq M_\infty \leq 25$)

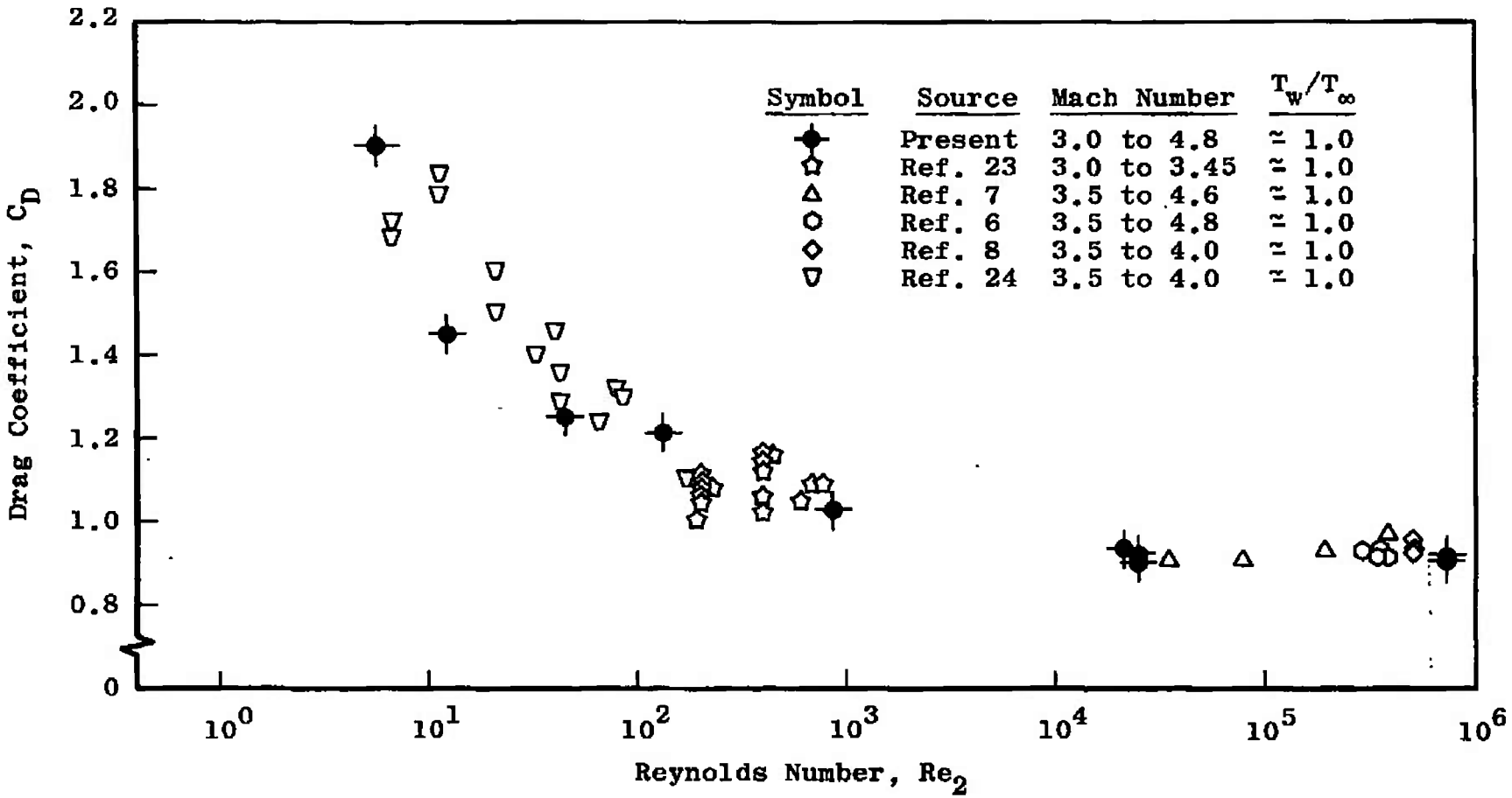

Fig. 7 Variation of Support-Free Sphere Drag Coefficient with Reynolds Number ($3 \leq M_\infty \leq 5$)

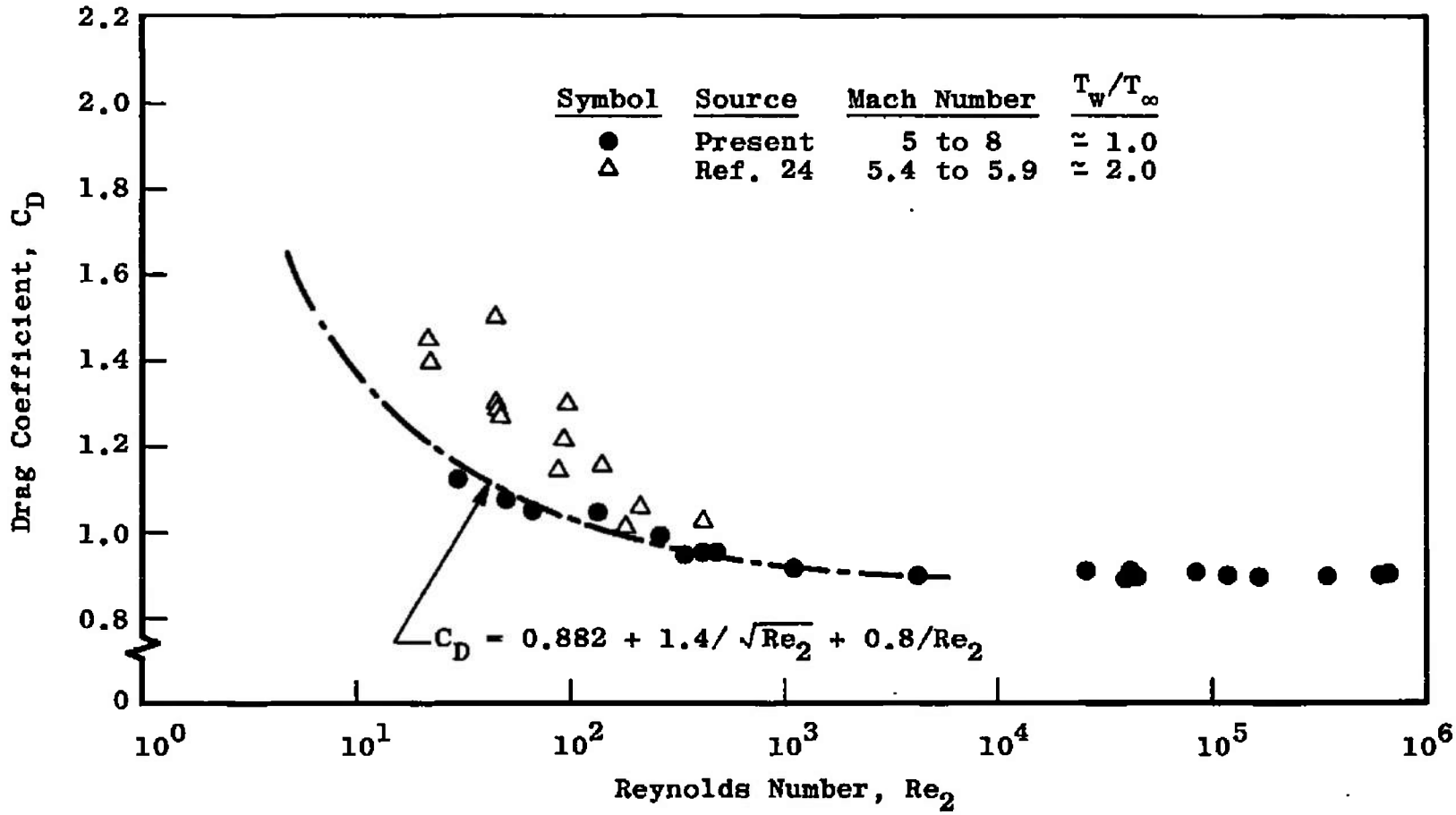

Fig. 8 Variation of Support-Free Sphere Drag Coefficient with Reynolds Number ($5 \leq M_\infty \leq 8$)

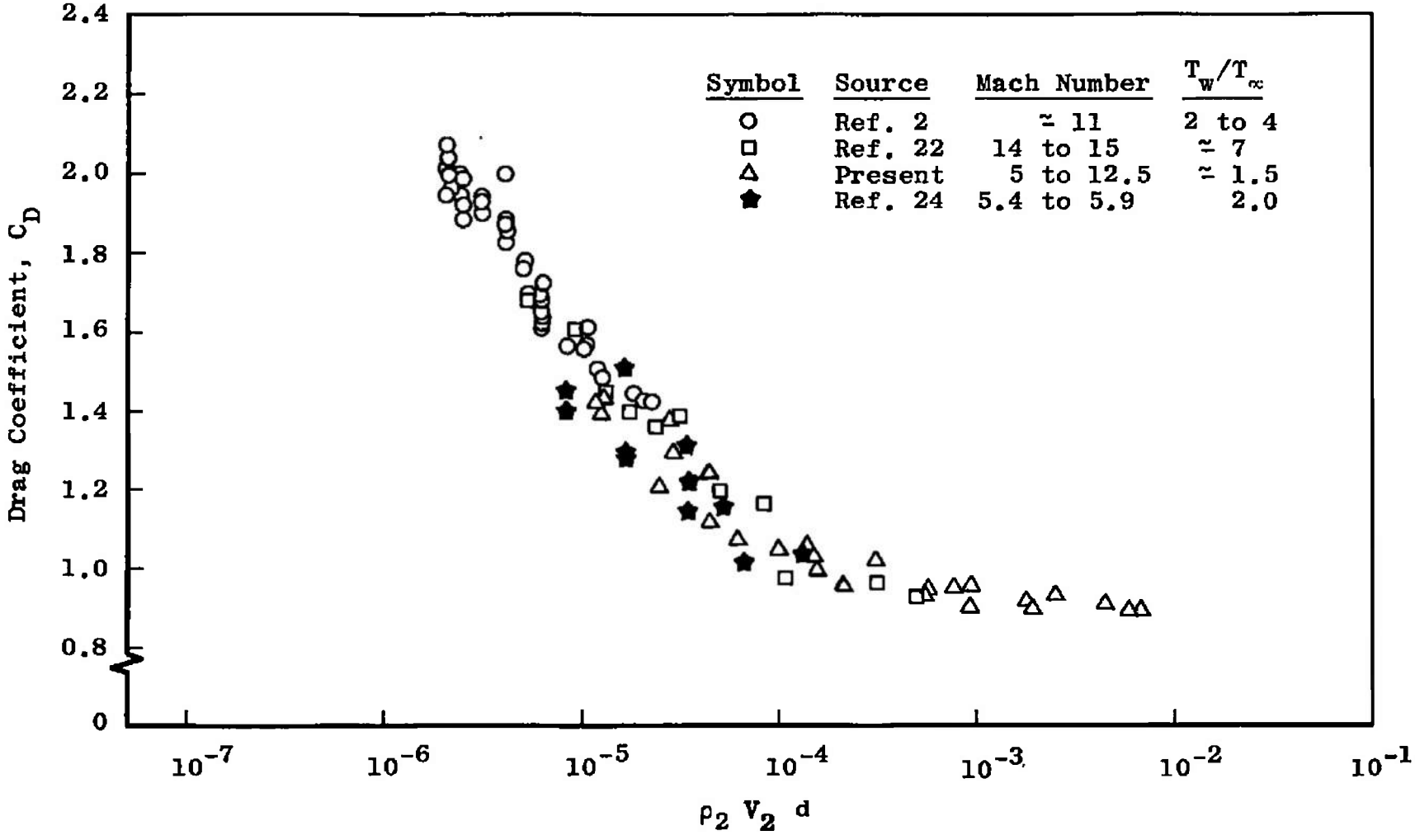

Fig. 9 Variation of Support-Free Sphere Drag Coefficient with $\rho_2 V_2 d$ ($5 \leq M_\infty \leq 15$)

TABLE I
PRESENT EXPERIMENTAL DATA

Shot No.	Diameter (in.)	Material	Velocity (ft/sec)	Re_∞	Re_2	C_D
716	0.250	Aluminum	3,178	43,936	24,850	0.941
718			4,739	55,805	22,270	0.924
722			5,269	72,163	26,280	0.907
723			5,403	74,506	26,700	0.900
724	0.401	Magnesium	5,864	128,860	42,980	0.904
725			7,761	171,592	45,060	0.893
726			8,251	160,065	39,950	0.889
727			7,485	144,870	39,040	0.903
728			10,017	183,121	40,710	0.882
743			2,910	70,065	43,110	0.966
744	0.250	Aluminum	3,105	48,025	27,650	0.966
746	0.437	Steel	12,636	303,520	58,120	0.879
747			16,134	341,775	52,950	0.871
786			9,995	284,170	62,510	0.876
787			13,362	274,350	50,830	0.896
802			10,686	473,702	99,390	0.893
803			12,407	530,760	101,000	0.895
804			12,211	531,134	102,460	0.901
809			6,780	583,322	123,840	0.890
810			6,684	575,340	123,420	0.886
811			7,720	664,050	176,210	0.887
812			7,726	667,230	177,050	0.885
813			9,494	817,640	184,650	0.884
814			9,480	835,080	188,970	0.886
815			10,207	440,010	95,350	0.879
816			10,794	463,280	96,540	0.891
818			6,455	278,660	84,720	0.909
820	0.401	Aluminum	8,797	171,500	41,040	0.887

TABLE I (Continued)

Shot No.	Diameter (in.)	Material	Velocity (ft/sec)	Re_∞	Re_2	C_D
821	0.401	Aluminum	8,520	169,700	41,570	0.893
826			9,333	33,920	8,032	0.867
828			10,672	50,360	11,070	0.873
829			10,532	40,420	8,970	0.875
830			12,766	50,210	9,996	0.883
832			15,676	57,280	9,340	0.871
833			15,771	60,330	9,802	0.881
834	0.437	Steel	10,542	900,550	188,830	0.907
835			11,070	956,570	193,800	0.892
888			14,044	1,206,030	207,610	0.889
892			12,152	1,047,650	200,210	0.892
894			14,779	641,645	106,430	0.889
898			15,314	684,131	109,740	0.887
899			13,785	1,164,320	203,090	0.879
900			15,159	643,430	103,970	0.879
902			16,017	348,890	54,630	0.877
905	0.437	Aluminum	15,731	156,590	25,300	0.872
906		Steel	7,892	1,335,090	345,410	0.886
909		Aluminum	13,463	45,668	8,581	0.869
911		Steel	8,449	1,438,460	352,950	0.888
912		Steel	9,098	1,501,220	346,850	0.891
914		Aluminum	17,046	173,120	26,110	0.876
915		Aluminum	14,015	55,094	9,987	0.867
916		Steel	15,904	336,710	52,860	0.902
920	0.938		7,035	2,665,070	758,160	0.889
921			7,786	2,871,100	748,120	0.892
922			8,841	3,242,300	769,750	0.904
926			8,594	3,050,690	739,700	0.893

TABLE I (Continued)

Shot No.	Diameter (in.)	Material	Velocity (ft/sec)	Re_∞	Re_2	C_D
927	0.437	Steel	15,718	336,370	53,560	0.878
928	0.437		15,764	340,710	54,010	0.882
930	0.938		8,839	3,119,300	739,700	0.890
931	0.437		14,152	615,760	106,000	0.877
933	0.437	Aluminum	14,071	139,172	24,765	0.898
934	0.437	Aluminum	13,206	123,045	23,460	0.873
938	0.437	Dylite	8,275	1,338	351	0.941
939	0.620	Hollow Steel	5,813	12,364	4,153	0.895
940	0.437	Dylite	6,641	899	272	0.988
949	0.375	Nylon	11,566	13,447	2,896	0.880
951	0.437	Steel	14,497	321,880	55,250	0.879
952	0.437	Steel	13,822	301,130	54,070	0.878
953	0.938	Steel	5,415	2,009,480	723,600	0.912
954	0.375	Nylon	11,524	12,540	2,724	0.882
956	0.938	Steel	5,374	2,001,120	719,570	0.908
986	0.375	Nylon	12,314	17,394	3,616	0.920
987	0.375	Nylon	11,685	19,872	4,228	0.888
1060	0.437	Aluminum	19,291	180,593	25,090	0.884
1065			19,052	189,363	26,156	0.881
1067			19,123	193,314	27,215	0.876
1068			19,274	195,892	27,384	0.876
1069			20,461	209,137	27,959	0.871
1070			18,996	190,162	26,878	0.874
1071			19,201	194,811	27,146	0.881
1073			19,118	196,148	27,383	0.881
1074			18,630	197,512	28,259	0.880
1075			19,099	186,793	26,087	0.881

TABLE I (Continued)

Shot No.	Diameter (in.)	Material	Velocity (ft/sec)	Re_∞	Re_2	C_D
1076	0.437	Aluminum	19,192	199,170	26,829	0.872
1078			19,348	204,727	28,363	0.879
1079			19,105	199,120	27,995	0.880
1077			19,052	184,241	26,772	0.887
1080			18,616	196,955	28,294	0.871
1081			18,344	187,125	26,920	0.889
1082			17,956	190,473	27,593	0.875
1083		Steel	12,249	109,727	20,530	0.885
1085			11,895	105,559	20,193	0.886
1086			12,228	109,608	20,502	0.880
1087			12,300	110,024	20,483	0.903
1088		Aluminum	12,445	109,695	20,612	0.891
1093		Aluminum	20,876	94,125	12,438	0.878
1117		Dylite	9,881	1,465	357	0.935
1119		Dylite	7,477	1,555	425	0.953
1120		Dylite	9,915	2,030	490	0.954
1121	0.375	Nylon	10,208	18,359	3,923	0.881
1122	0.375	Nylon	10,267	15,658	3,560	0.857
1123	0.250	Nylon	9,832	6,939	1,509	0.930
1124	0.250	Nylon	9,865	5,234	1,275	0.890
1127	0.437	Dylite	9,412	588	146	0.955
1128	0.437	Dylite	9,470	452	97	0.990
1133	0.437	Dylite	9,558	2,508	607	0.957
1139	0.250	Nylon	8,743	4,545	1,148	0.915
1140	0.437	Dylite	9,311	260	67	1.042
1141	0.437	Dylite	6,958	167	50	1.073
1143	0.437	Dylite	9,226	120	30	1.120
1145	0.250	Dylite	9,634	45	12	1.150

TABLE I (Concluded)

Shot No.	Diameter (in.)	Material	Velocity (ft/sec)	Re_∞	Re_2	C_D
1146	0.250	Nylon	10,361	11,758	2,557	0.907
1147	0.250	Dylite	10,357	117	29	1.240
1148	0.250	Dylite	10,104	80	20	1.290
1153	0.437	Dylite	9,978	414	103	1.030
1154	0.250	Dylite	11,176	75	18	1.370
1155	0.250	Dylite	9,673	87	23	1.260
1161	0.125	Nylon	3,288	277	145	1.200
1162	0.125	Dylite	3,187	9.8	5.3	1.930
1163	0.125	Nylon	5,894	402	132	1.042
1167	0.437	Dylite	11,894	358	78	1.060
1168	0.125	Nylon	10,116	845	197	1.020
1169	0.125	Dylite	10,706	34	8.4	1.390
1170	0.125	Dylite	10,621	31	7.6	1.420
1171	0.125	Dylite	10,186	36	9.0	1.430
1173	0.125	Dylite	3,321	88	45	1.250
1174	0.250	Nylon	3,383	1,720	871	1.025
1175	0.250	Dylite	9,847	65	16	1.200
1176	0.250	Dylite	3,246	24	13	1.450

APPENDIX I
RANGE K

LAUNCHER

All of the models used in this series of tests were sabot launched. Two basic types of sabots were used (Fig. I-2): (1) aerodynamic type, where aerodynamic forces are used to separate the model and the split sabot; and (2) pusher type, where the model and sabot are separated by mechanical means. The mechanical strippers are two-stage devices. The first stage consists of a series of pins which interfere with the sabot and provide initial separation of model and sabot. The second stage can be an annular lead ring which stops the sabot, or an angled ramp which deflects the sabot onto a catcher plate in the blast tank. Of the two types of mechanical stripping, the angled ramp seems to have been the most successful in providing a clean launch in these tests.

The launcher is a two-stage, light-gas gun consisting of a powder chamber, pump tube, high-pressure section, and launch tube. The powder chamber and pump tube can be used in conjunction with a variety of high-pressure sections and launch tubes having internal diameters ranging from 0.5 to 1.0 in. An idea of the velocity capability of this launcher as a function of in-gun weight is given in Fig. I-1. When particular attention is given to repeating the launch velocity, it has been shown that this can be achieved to an accuracy of ±2 percent, up to velocities on the order of 20,000 ft/sec.

BLAST AND RANGE TANKS

Both of these tanks are 6-ft-diam cylinders connected by a short spool piece containing a high-vacuum valve which permits the isolation of the two tanks. The blast tank is 12 ft long and has a series of ports along the sides and upper surface which permit the X-ray photography of the model as it leaves the muzzle of the launcher and flies through the blast tank. At the downrange end of this tank is an easily removable thick plate with a 2-in.-diam hole through which the model flies. This plate acts as a stop for the sabot, a restrictor in the flow of muzzle gas into the range, and, finally, minimizes the effect of muzzle flash on the instrumentation in the range tank.

The range tank is 103 ft long and is equipped with six dual-axis shadowgraph stations installed at approximately 15-ft intervals. This system, wholly external to the range tank except for the plastic Fresnel lenses, was designed primarily to photograph the position and attitude of models.

VACUUM SYSTEM

The vacuum system consists of mechanical roughing pumps, a Roots blower, and an oil diffusion pump. The blast and range tanks have independent pumping systems which facilitate testing at low pressures because the range tank can be kept at a very low pressure (≈0.05 mm Hg) while the launcher is being prepared for the next launching. A pressure on the order of 0.001 mm Hg has been achieved in the range tank alone with an apparent leak rate of 0.0005 mm Hg/min. This may not be a realistic value for the leak rate because of the relatively short pumpdown time for this particular test, i.e., outgassing may have obscured the actual leak rate.

TEMPERATURE MEASUREMENT

Gas temperature in the range tank is measured with copper-constantan thermocouple probes located at four stations along the length of the range tank. An assessment of the possible errors has indicated that an accuracy of approximately ±0.5 percent of the absolute temperature (approximately 294°K) is possible with this system.

PRESSURE MEASUREMENT

All gages used to measure pressure in the range tank are connected to a large stainless steel manifold which can be isolated from the range tank and kept under high vacuum when not in use. The valve isolating this manifold from the range tank is opened before a test, and the pressure is monitored on the relevant gages until 15 sec before firing, at which time the valve is closed. With this technique any pressure measuring errors caused by the apparent leak rate are minimized. This problem is of greatest significance at the lower pressures, i.e., below 1.0 mm Hg. Six pressure gages can be connected to the manifold, and each gage station has a system of vacuum valves whereby the gage can be moved without disturbing the rest of the system.

At this time, three gages are used to measure pressure from atmospheric to the order of 0.030 mm Hg:

1. Hass Mercury Manometer - This instrument is used over the pressure range from 15 to 760 mm Hg. It has a resolution of 0.05 mm Hg and an accuracy of ±0.22 mm Hg. This implies an accuracy of ±1.5 percent at 15 mm Hg, an amount which experience has shown to be a maximum error rather than one which is normally encountered.

2. Micromanometer - This is an oil-filled, U-tube manometer based on one designed for the low-density wind tunnel at Berkeley, California (Ref. 26). Considerable experience has been gained with this type of instrument at the VKF low-density hypersonic wind tunnel (Gas Dynamic Wind Tunnel, Hypersonic (L)), where it is used to calibrate pressure transducers (Ref. 27). The resolution of this instrument is approximately 0.0015 mm Hg. At a pressure of approximately 15 mm Hg where this instrument overlaps the Hass gage, the agreement between the two instruments is on the order of 0.5 percent.

3. Baratron - This is a variable capacitance pressure transducer having a small internal volume. The volume of the above two instruments is large, and, consequently, at low pressures they do not respond as rapidly as the Baratron to a changing pressure. The Baratron used at AEDC has two sensing heads rated at 30 and 1000 mm Hg. This permits the measurement of pressure from atmospheric down to pressures on the order of 0.030 mm Hg. A static comparison of these two heads with the Hass gage and the micromanometer over the pressure range from 0.5 to 760 mm Hg indicates an agreement of better than 1 percent. Below 0.1 mm Hg the resolution of the micromanometer is not sufficient to make a really accurate comparison with the Baratron; however, the indications are that the Baratron gives consistent pressure readings at pressures as low as 0.030 mm Hg. Essentially, the same transducer calibration technique as described in Ref. 27 is used here. It is perhaps worth noting here that at this time there is no standard available from the National Bureau of Standards for pressures less than 1 mm Hg.

An error in pressure measurement at low pressures can occur if there is a temperature difference between the pressure transducer and the position where the pressure is sensed. This is the thermal transpiration effect discussed in Ref. 28. It has been noted that a temperature difference between the range and the pressure transducer of 10°F can occur. If it is assumed that the flow in the sensing tube is in the free-molecule flow regime, such a temperature difference would cause a 1-percent error in the pressure measurement. Since for the present series of tests the flow is closer to the continuum regime, the pressure error caused by this temperature difference can safely be ignored.

MODEL DETECTION

Each orthogonal shadowgraph station has two detectors, as described below:

1. Shadow detector - With this type, the model passes through a light beam shining from one side of the range onto a phototransistor. The passage of the model through this beam causes an electrical output pulse from the phototransistor which is used to trigger the shadowgraph spark source which, in turn, triggers the station chronograph.

2. Radiation detector - With this detector the naturally occurring model radiation has to be sufficient to be sensed by a phototransistor which then triggers the station spark source.

There are regions of overlap in range operation where either detector will detect a particular model. When it is not absolutely certain which mode of operation will detect a model in a particular test, both detectors are turned on. At this time the shadow mode detector has successfully detected 0.125-in.-diam spheres up to velocities of 16,000 ft/sec, whereas the radiation detector has successfully detected a 0.125-in.-diam sphere at 29,000 ft/sec.

VELOCITY MEASURING SYSTEM

Shadowgrams of the model are obtained for each of the six orthogonal shadowgraph stations. The position of the sphere with respect to the local shadowgraph origin, and hence relative to the master axis system, is determined. The timing intervals corresponding to the above distances are measured with chronographs operating off a common, 10-mc time base. At least ten of these chronographs were used on each firing; five were used to measure the single-station interval, and the others were used to measure the time interval for multiple-station intervals. In this way the deleterious effect of a single counter malfunction can be minimized. It has been demonstrated that the existing system has a velocity measuring accuracy of ±0.03 percent for the range of velocities considered herein.

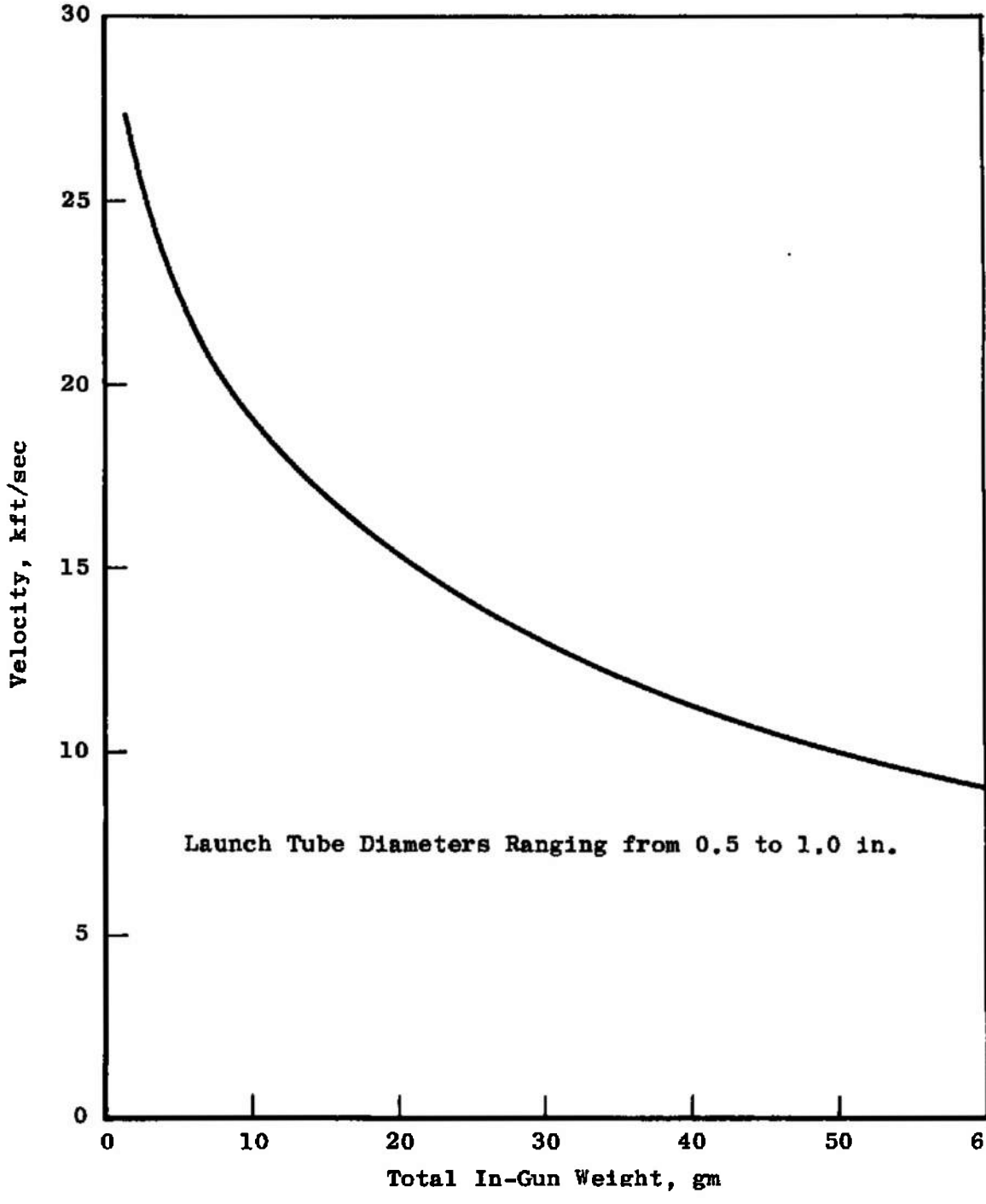

Fig. I-1 Operational Capability of the Range K Two-Stage Light-Gas Gun (1965)

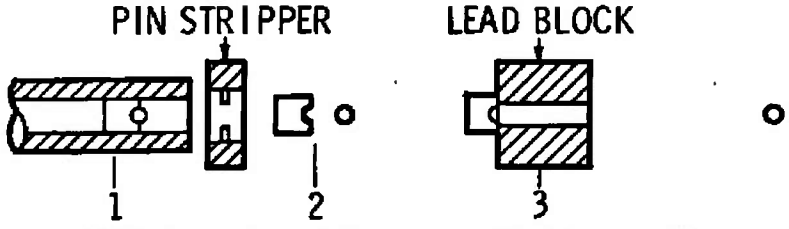

1. MODEL AND SABOT TOGETHER IN LAUNCH TUBE.
2. MODEL AND SABOT SEPARATED AFTER PASSING THROUGH PIN STRIPPER.
3. SABOT ARRESTED BY LEAD BLOCK - MODEL PASSES THROUGH A HOLE IN THE BLOCK AND ON DOWN RANGE.

PIN AND LEAD ORIFICE STRIPPER

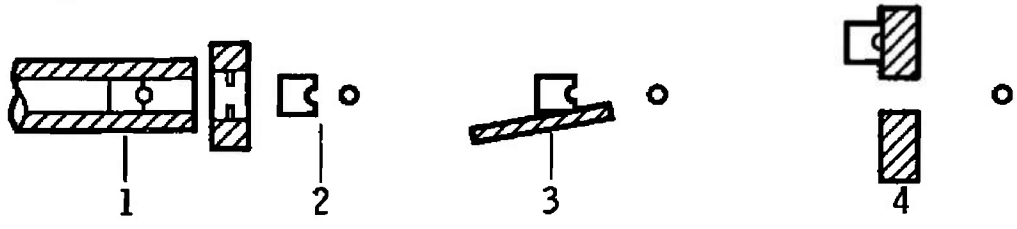

1.-2. AS ABOVE.
3. SABOT STRIKES ANGLED RAMP AND DEFLECTS VERTICALLY.
4. SABOT STRIKES CATCHER PLATE - SPHERE PASSES THROUGH HOLE AND ON DOWN RANGE.

PIN AND RAMP STRIPPER

1. MODEL AND SABOT TOGETHER IN LAUNCH TUBE.
2. PETALLED SABOT SPREADING UNDER ACTION OF AERODYNAMIC FORCES.
3. SABOT ARRESTED BY CATCHER PLATE - SPHERE PASSES THROUGH HOLE AND ON DOWN RANGE.

AERODYNAMIC STRIPPER

Fig. I-2 Model Separation Techniques Used in Range K

UNCLASSIFIED
Security Classification

DOCUMENT CONTROL DATA - R&D

(Security classification of title, body of abstract and indexing annotation must be entered when the overall report is classified)

1. ORIGINATING ACTIVITY (Corporate author) Arnold Engineering Development Center ARO, Inc., Operating Contractor Arnold Air Force Station, Tennessee	2a. REPORT SECURITY CLASSIFICATION UNCLASSIFIED 2b. GROUP N/A

3. REPORT TITLE
SPHERE DRAG MEASUREMENTS IN AN AEROBALLISTICS RANGE AT HIGH VELOCITIES AND LOW REYNOLDS NUMBERS

4. DESCRIPTIVE NOTES (Type of report and inclusive dates)
N/A

5. AUTHOR(S) (Last name, first name, initial)
Bailey, A. B., ARO, Inc.

6. REPORT DATE May 1966	7a. TOTAL NO. OF PAGES 44	7b. NO. OF REFS 28
8a. CONTRACT OR GRANT NO. AF 40(600)-1200 b. ~~PROJECT NO.~~ Program Element 65402234 c. d.	9a. ORIGINATOR'S REPORT NUMBER(S) AEDC-TR-66-59 9b. OTHER REPORT NO(S) (Any other numbers that may be assigned this report) N/A	

10. AVAILABILITY/LIMITATION NOTICES
Qualified users may obtain copies of this report from DDC.

11. SUPPLEMENTARY NOTES N/A	12. SPONSORING MILITARY ACTIVITY Arnold Engineering Development Center Air Force Systems Command Arnold Air Force Station, Tennessee

13. ABSTRACT

The drag coefficients of spheres for $Re_2 > 10^4$ have been measured in the velocity range $3000 \lesssim V_\infty \lesssim 21,000$ ft/sec with an accuracy of approximately ± 1.5 percent. In addition, successful techniques for manufacturing and launching ultralightweight spheres (densities approaching 1 lb/ft^3) have resulted in the ability to measure sphere drag coefficient in the velocity range $3000 \lesssim V_\infty \lesssim 12,000$ ft/sec and Reynolds number range $3 \lesssim Re_2 \lesssim 10^6$, with an accuracy of approximately ± 4 percent. This wide range of operating conditions has made it possible to study the initial departures of sphere drag coefficient from the high Reynolds number, continuum level and also to make measurements at free-stream Knudsen numbers approaching 1.0. The results of the tests at the low Reynolds numbers are shown to be consistent with the results obtained in other low-density, hypersonic-flow facilities. (U)

DD FORM 1 JAN 64 1473

UNCLASSIFIED
Security Classification

14 KEY WORDS	LINK A ROLE	LINK A WT	LINK B ROLE	LINK B WT	LINK C ROLE	LINK C WT
sphere drag measurements						
ultralight projectiles						
hypersonic flow						

INSTRUCTIONS

1. ORIGINATING ACTIVITY: Enter the name and address of the contractor, subcontractor, grantee, Department of Defense activity or other organization *(corporate author)* issuing the report.

2a. REPORT SECURITY CLASSIFICATION: Enter the overall security classification of the report. Indicate whether "Restricted Data" is included. Marking is to be in accordance with appropriate security regulations.

2b. GROUP: Automatic downgrading is specified in DoD Directive 5200.10 and Armed Forces Industrial Manual. Enter the group number. Also, when applicable, show that optional markings have been used for Group 3 and Group 4 as authorized.

3. REPORT TITLE: Enter the complete report title in all capital letters. Titles in all cases should be unclassified. If a meaningful title cannot be selected without classification, show title classification in all capitals in parenthesis immediately following the title.

4. DESCRIPTIVE NOTES: If appropriate, enter the type of report, e.g., interim, progress, summary, annual, or final. Give the inclusive dates when a specific reporting period is covered.

5. AUTHOR(S): Enter the name(s) of author(s) as shown on or in the report. Enter last name, first name, middle initial. If military, show rank and branch of service. The name of the principal author is an absolute minimum requirement.

6. REPORT DATE: Enter the date of the report as day, month, year; or month, year. If more than one date appears on the report, use date of publication.

7a. TOTAL NUMBER OF PAGES: The total page count should follow normal pagination procedures, i.e., enter the number of pages containing information.

7b. NUMBER OF REFERENCES: Enter the total number of references cited in the report.

8a. CONTRACT OR GRANT NUMBER: If appropriate, enter the applicable number of the contract or grant under which the report was written.

8b, 8c, & 8d. PROJECT NUMBER: Enter the appropriate military department identification, such as project number, subproject number, system numbers, task number, etc.

9a. ORIGINATOR'S REPORT NUMBER(S): Enter the official report number by which the document will be identified and controlled by the originating activity. This number must be unique to this report.

9b. OTHER REPORT NUMBER(S): If the report has been assigned any other report numbers *(either by the originator or by the sponsor)*, also enter this number(s).

10. AVAILABILITY/LIMITATION NOTICES: Enter any limitations on further dissemination of the report, other than those imposed by security classification, using standard statements such as:

(1) "Qualified requesters may obtain copies of this report from DDC."

(2) "Foreign announcement and dissemination of this report by DDC is not authorized."

(3) "U. S. Government agencies may obtain copies of this report directly from DDC. Other qualified DDC users shall request through _____."

(4) "U. S. military agencies may obtain copies of this report directly from DDC. Other qualified users shall request through _____."

(5) "All distribution of this report is controlled. Qualified DDC users shall request through _____."

If the report has been furnished to the Office of Technical Services, Department of Commerce, for sale to the public, indicate this fact and enter the price, if known.

11. SUPPLEMENTARY NOTES: Use for additional explanatory notes.

12. SPONSORING MILITARY ACTIVITY: Enter the name of the departmental project office or laboratory sponsoring *(paying for)* the research and development. Include address.

13. ABSTRACT: Enter an abstract giving a brief and factual summary of the document indicative of the report, even though it may also appear elsewhere in the body of the technical report. If additional space is required, a continuation sheet shall be attached.

It is highly desirable that the abstract of classified reports be unclassified. Each paragraph of the abstract shall end with an indication of the military security classification of the information in the paragraph, represented as *(TS)*, *(S)*, *(C)*, or *(U)*.

There is no limitation on the length of the abstract. However, the suggested length is from 150 to 225 words.

14. KEY WORDS: Key words are technically meaningful terms or short phrases that characterize a report and may be used as index entries for cataloging the report. Key words must be selected so that no security classification is required. Identifiers, such as equipment model designation, trade name, military project code name, geographic location, may be used as key words but will be followed by an indication of technical context. The assignment of links, rules, and weights is optional.